Adaptation Kinetics in Bacterial Chemotaxis

JOURNAL OF BACTERIOLOGY, Apr. 1983, p. 312-323
0021-9193/83/040312-12$02.00/0

Vol. 154, No. 1

Adaptation Kinetics in Bacterial Chemotaxis

STEVEN M. BLOCK, JEFFREY E. SEGALL, AND HOWARD C. BERG*

Division of Biology, California Institute of Technology, Pasadena, California 91125

Received 18 October 1982/Accepted 21 January 1983

Cells of *Escherichia coli*, tethered to glass by a single flagellum, were subjected to constant flow of a medium containing the attractant α-methyl-DL-aspartate. The concentration of this chemical was varied with a programmable mixing apparatus over a range spanning the dissociation constant of the chemoreceptor at rates comparable to those experienced by cells swimming in spatial gradients. When an exponentially increasing ramp was turned on (a ramp that increases the chemoreceptor occupancy linearly), the rotational bias of the cells (the fraction of time spent spinning counterclockwise) changed rapidly to a higher stable level, which persisted for the duration of the ramp. The change in bias increased with ramp rate, i.e., with the time rate of change of chemoreceptor occupancy. This behavior can be accounted for by a model for adaptation involving proportional control, in which the flagellar motors respond to an error signal proportional to the difference between the current occupancy and the occupancy averaged over the recent past. Distributions of clockwise and counterclockwise rotation intervals were found to be exponential. This result cannot be explained by a response regulator model in which transitions between rotational states are generated by threshold crossings of a regulator subject to statistical fluctuation; this mechanism generates distributions with far too many long events. However, the data can be fit by a model in which transitions between rotational states are governed by first-order rate constants. The error signal acts as a bias regulator, controlling the values of these constants.

Bacteria respond in a transient manner to abrupt changes in their environment: they adapt. When exposed to a large stepwise increase in the concentration of an attractant (or decrease in the concentration of a repellent), cells swim smoothly (or, if tethered, rotate counterclockwise [CCW]) for minutes before resuming their normal mode of behavior (6, 19, 20, 28, 29). When exposed to a large stepwise increase in the concentration of a repellent (or decrease in the concentration of an attractant), they tumble (or rotate clockwise [CW]) for several seconds before recovery. These responses are asymmetric: the flagellar motors remain in the CCW mode much longer than in the CW mode. Recovery times (28) or transition times (6) are proportional to the net change in the occupancy of specific chemoreceptors. The stimuli used in these experiments saturate the sensory system: they are much larger than stimuli encountered in nature, in which bacteria swim slowly through spatial gradients that have been smoothed by diffusion. Chemotaxis evolved under the latter condition. It is important, therefore, to define the properties of the chemosensory system in the small-signal domain.

It was evident from tracking cells in spatial gradients of L-aspartate and L-serine (5) that the run (or CCW) bias increases when cells swim in favorable directions, but it was not possible to characterize the response accurately over a wide dynamic range. When cells are uniformly distributed in an exponential gradient of L-serine, they move up the gradient with a uniform migrational velocity, indicating a net response proportional to the spatial change in the logarithm of concentration, $d(\log C)/dx$ (10, 11). Data from cells tracked in spatially isotropic temporal gradients of L-glutamate indicate a response proportional to the time rate of change of chemoreceptor occupancy (9). At concentrations near the dissociation constant of the chemoreceptor, this reduces to a response proportional to the temporal change in the logarithm of concentration, $d(\log C)/dt$. Over a broader range, it explains results obtained from sensitivity assays, in which the number of cells swimming from a pond into a capillary tube containing attractant at a fixed concentration ratio varies with the concentration (22).

Recently, we measured the response of tethered cells to short iontophoretic pulses of attractants and repellents (8). The impulse response has a finite width, indicating that cells integrate

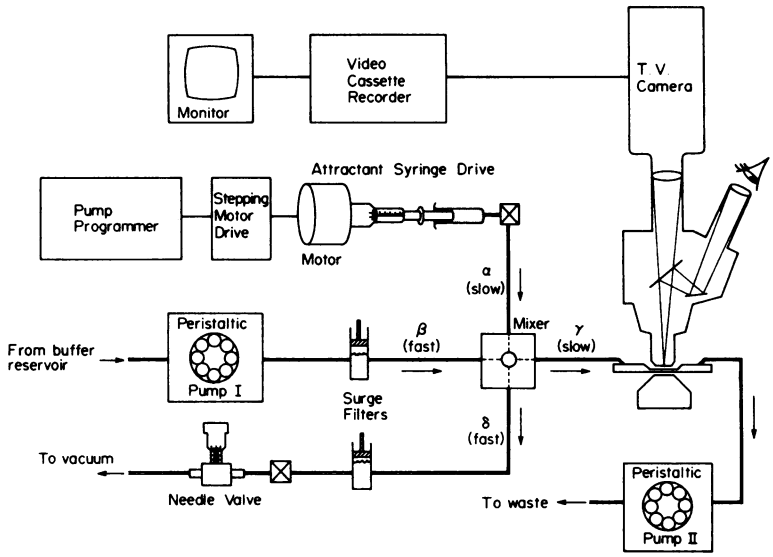

FIG. 1. Apparatus for subjecting tethered cells to programmed changes in concentration. A concentrated solution of attractant was combined with buffer in a small mixing chamber. Part of the mixture was passed through a flow chamber holding the tethered bacteria, and the rest was collected in a trap in a vacuum line (not shown). The concentration of attractant was controlled with a programmed pump. Other flow rates were adjusted to give linearity in the mixing and a fast mixing time, with the flow past the cells held constant.

sensory inputs over a period of a few seconds. It also is biphasic, indicating that the cells take time derivatives of these inputs. The sensory system is maximally tuned to concentration changes that occur over a span of about 4 s, an interval over which changes normally occur when cells swim in spatial gradients.

Do bacteria, in fact, continually compute and respond to the time derivative of their chemoreceptor occupancy? How might they do so? Previous work on temporal stimulation of free-swimming bacteria was limited to measurements made for a short period of time on a large number of different cells whose responses varied widely. The tethered-cell approach offers the possibility of sustained observation of the responses of one cell to different, precisely defined, stimuli. The large amount of data that can be collected in this manner permits more rigorous tests of models of flagellar behavior.

In the experiments described here, we exposed tethered cells to gradual changes in the concentration of a non-metabolizable attractant, α-methyl-DL-aspartate (21). The results complement and extend those obtained from measurements of the impulse response. Changes in rotational bias can be accounted for by a model for adaptation in which an error signal, proportional to the difference between the current receptor occupancy and the occupancy averaged over the recent past, modulates the probabilities for transitions between discrete flagellar states.

MATERIALS AND METHODS

Reagents. α-Methyl-DL-aspartate was obtained from Sigma Chemical Co. All other amino acids (A grade) were obtained from Calbiochem. Lactic acid (reagent grade) came from Mallinckrodt, and EDTA came from Fisher Scientific Co.

Tethered cells. Wild-type *Escherichia coli* AW405 (2) was grown and tethered as described by Block et al. (8), except that the motility medium was 0.067 M NaCl–0.01 M potassium phosphate (pH 7.0)–0.01 M sodium lactate–10^{-4} M EDTA–10^{-6} M L-methionine. The anti-filament antibody was preadsorbed against a *hag* derivative of strain AW405.

Apparatus. A stainless steel flow cell holding a cover slip with tethered cells was placed on a temperature-regulated stage (32.0°C) of an inverse phase-contrast microscope (Nikon S-Ke; magnification, 400×) as shown in Fig. 1. The buffer reservoir was also held at 32.0°C. Images of the cells were recorded with a video camera (Sanyo VC1620X, 2:1 interlace) and cassette recorder (Sanyo VTC7100) and displayed on a 23-cm monitor (Hitachi VM910). The amount of attractant reaching the cells was controlled by a pump (adapted from a Radiometer SBU1 syringe burette) driven by a stepping motor (Rapid-Syn 23H-05A) controlled by an electronic programmer built for the purpose. This pump fed a concentrated solution of attractant (4×10^{-3} M α-methyl-DL-aspartate in motility medium) to a small mixing chamber (a Plexiglass cylinder 0.09 ml in volume packed with glass wool 0.5 μm in diameter) at a variable rate, α. Connections were made with polyethylene tubing (inside diameter, 0.58 mm) and sections of stainless steel needles (22 gauge). A 12.5-cm length of polyethylene tubing connected the mixer to the flow cell, which had an internal

volume of about 0.05 ml. The flow rates β and γ were generated by peristaltic pumps I and II, which comprised different pumping tubes on a four-stage head of a Gilson Minipuls II; for all experiments, β and γ were fixed at 0.028 and 0.0032 ml/s, respectively, the latter level being low enough to allow free rotation of the tethered cells. Small surges in pumping speed arising from roller-to-roller changes were suppressed with surge filters made from 3-ml syringe bodies: the air cavities could be tuned by sliding the plungers in or out. The excess fluid was carried away at the rate $\delta = (\alpha + \beta - \gamma) \simeq 10\gamma$ by a vacuum line via a needle valve adjusted to maintain a slight negative pressure at the flow cell, which ensured that the cover slip maintained a proper seal. To prevent air bubbles from destroying the preparation, the solutions used in the experiment were autoclaved and then saturated with a mixture of 80% He–20% O_2.

When α is constant, the concentration of attractant in the flow cell is $C = C_\alpha\alpha/(\alpha + \beta)$ where C_α is the concentration of attractant in the syringe. If $\beta \gg \alpha$, then $C = C_\alpha\alpha/\beta$, and the concentration is proportional to α. The values used for α ranged from about 0.0003 to 0.0035 ml/s, giving a worst-case mixing nonlinearity of 11%. The mixer behaves as a low-pass filter for concentration according to the relation $dC/dt = (\alpha C_\alpha - \beta C)/V$, where V is the effective volume of the mixer. When α changes abruptly, C slews exponentially to a new value with a mixing time constant $\tau_{mix} = V/\beta = 11$ s. This constant was determined experimentally by varying α sinusoidally and measuring the phase and amplitude of the changes in concentration at the output. The calibration was done by replacing the attractant with methylene blue, placing an orange band-pass filter in front of the microscope lamp to enhance contrast, and replacing the video camera with a photodiode (United Detector Technology PIN6), which converted the microscope into a microspectrophotometer. As a final check to ensure that the system was free of surges of concentration and that mixing was complete, the apparatus was converted to its normal configuration, and adjacent tethered cells were followed at fixed α. Variations in concentration above threshold would be expected to result in cross-correlated rotational behavior. No such correlation was observed.

Data acquisition. For measurements of rotational bias, the video tapes were played back at quarter speed while an operator scored rotational periods by eye, holding a push button down for CW events and releasing it for CCW events. This button toggled an event marker on a strip-chart recorder running at 5 mm/s. Strip charts were digitized (8), and the data, a list of numbers representing the times of CW-to-CCW or CCW-to-CW transitions, were stored as records in a PDP 11/34 computer for subsequent analysis. The accuracy of the method was checked by slightly displacing the image of a spinning cell up or down at exponentially distributed random times, with the operator scoring up as CW and down as CCW. Interval distributions computed from these records were nearly exponential, but as expected, operators tended to miss or stretch the shortest events. This effect was significant only for intervals in operator time of less than 0.6 s, which scales to a real time of 0.15 s owing to the quarter-speed playback. The resolution for real-time intervals longer than 0.4 s was better than 0.05 s. For measurements of angular velocity, the tapes were played back into a system linked to an Apple computer that timed pulses generated whenever the image of a rotating cell crossed a video cursor.

Data analysis. CW or CCW interval distributions were constructed by sorting intervals into bins and counting the number of events in each bin. In the interest of learning whether these distributions were exponential, as suggested by earlier work (6), we combined data from different cells obtained either before or during ramps. If the distribution for each cell is exponential, then it is possible to combine data from different cells systematically by normalizing the intervals of each cell to the mean for that cell. This produces another exponential distribution, a distribution of unit mean, which can be added to (i.e., binned together with) normalized distributions derived from other cells. Such a procedure relies on the fact that all exponential distributions are identical up to a scaling factor. The final global distribution can be rescaled to yield a plot with a mean equal to the average of the means of the original distributions.

Unfortunately, as noted above, the finite resolution of the digitizing technique limited our ability to record the shortest intervals with high fidelity. Therefore, events lasting less than 0.4 s were eliminated from each histogram, and a mean was computed from the remaining intervals. This mean was adjusted downwards by 0.4 s to compensate for the cutoff (a procedure that yields an accurate mean for any exponential distribution). The remaining intervals were scaled to the adjusted mean, combined with normalized data from other cells in a histogram containing 100 bins, and rescaled to yield a plot with a mean equal to the average of the adjusted means of the original distributions. This plot was tested for exponentiality by a nonlinear least-squares program (7) that returned a value for the reduced χ^2 (χ^2 divided by the number of degrees of freedom). This allowed a test of the hypothesis that the parent distribution, the distribution from which the data for each cell were derived, was exponential (for intervals exceeding 0.4 s). The corresponding probability (P) value is an estimate of the probability that a reduced χ^2 of that value or greater would be expected to occur by chance. In making this test, bins were ignored for intervals extending out to about 1 s. When a truncated record with a relatively small adjusted mean is scaled upwards, no contribution is made to bins corresponding to times equal to 0.4 s times the scale factor, which can be a number greater than 1; therefore, the final distribution is anomalous for bins corresponding to times even longer than 0.4 s.

The probability of CCW rotation was estimated by calculating the fraction of time that a cell spent rotating CCW. For computing values of this parameter for periods before or during ramps, the time that the cell spent rotating CCW in the period of interest was divided by the total time in that period. For looking at variations in this fraction as a function of time, the following procedure was used. First, the total time spent CCW up to a given reversal was computed. This sum, considered as a function of t, has a time derivative (slope) constrained to lie between 0 (if the cell spun exclusively CW) and 1 (if the cell spun exclusively CCW). The derivative provides a measure, at time t, of the fraction of time spent spinning CCW. The sum was computed and then digitally filtered with a cubic

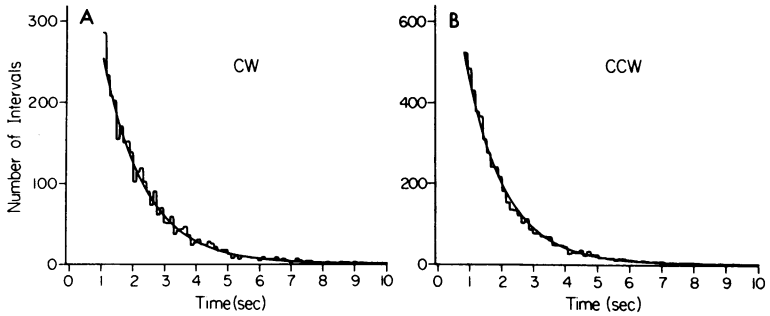

FIG. 2. CW and CCW interval distributions of adapted cells. Histograms for each record were scaled, combined, and fit by an exponential, as described in the text. (A) CW interval distribution computed from the 5,237 events longer than 0.4 s in 108 records on 24 cells; 4 events are off the scale. Range of adjusted means for each record, 0.14 to 4.4 s; global adjusted mean, 1.06 s; decay time for the exponential fit, 1.33 s; reduced χ^2, 1.06; 51 degrees of freedom; P value, 36%. (B) CCW interval distribution computed from the 7,255 events longer than 0.4 s in 108 records on 24 cells; 13 events are off the scale. Range of adjusted means for each record, 0.47 to 5.2 s; global adjusted mean, 1.20 s; decay time for the exponential fit, 1.22 s; reduced χ^2, 1.05; 54 degrees of freedom; P value, 37%.

spline-fit smoothing routine (24, 25), which smooths the fit curve in a least-squares sense and generates coefficients that define the derivative. For the derivative to be well behaved, the smoothing must span several adjacent rotation intervals. Thus, although the derivative provides an estimate of the rotational bias at time t, its value depends on the behavior of the cell at adjacent times. As a result, abrupt changes in bias are rounded off.

The reversal rate was computed from the density of data points, as described by Block et al. (8). The Montecarlo simulation of the response-regulator model was done by arranging for a counter (representing the amount of regulator, X) to be incremented by one exponential process and decremented by another, with probabilities obtained from random-number generation. The program kept track of those intervals for which the counter was above or below a critical value (corresponding to X_{crit}) and compiled the corresponding interval histograms.

RESULTS

It is known from earlier work with free-swimming cells (9–11, 22, 28) that *E. coli* is maximally sensitive to an attractant at a concentration equal to the apparent dissociation constant of its chemoreceptor, K_D. For α-methyl-DL-aspartate, $K_D \simeq 1.4 \times 10^{-4}$ M (6, 22). At an attractant concentration C, the fraction of receptor bound is $P = C/(K_D + C)$, and the time rate of change of this fraction is $dP/dt = [K_D C/(K_D + C)^2] \times (dC/dt)/C$. The term in square brackets is a bell-shaped function centered at K_D, the factor measured in sensitivity assays (9, 22). By limiting changes in concentration to a range logarithmically centered around K_D, from $C_{low} = 0.31\ K_D$ to $C_{high} = 3.2\ K_D$, the variation in this factor is reduced to less than 20% about the mean, and $dP/dt \simeq \frac{1}{4}(dC/dt)/C = \frac{1}{4}d(\log C)/dt$. If the response of the cells is proportional to dP/dt, then it should be linear in the logarithm of concentration, a type of behavior specified by the Weber-Fechner law (11). We tested exponential ramps of the form $\exp(at)$, with ramp rates, a, of either sign, and exponentiated sine waves of the form $\exp[\sin(\omega t)]$. These stimuli generate changes in P that are linear and sinusoidal, respectively.

Behavior at fixed concentration. The cells were allowed to adapt to C_{low} or C_{high} for at least 5 min before data were taken. They were monitored for 3 to 5 min before and immediately after each ramp. The interval distributions for data obtained before the ramps are shown in Fig. 2. These distributions were accurately fit by single exponentials. The interval distributions at C_{low} were indistinguishable from those at C_{high} (data not shown), indicating that the cells fully adapt.

The cells were continuously perfused with buffer containing lactate (an energy source [1]) and L-methionine (required for adaptation in cells that do not synthesize it [27]). They were well oxygenated but deprived of other amino acids and nutrients. The cells continued to rotate and respond for at least 6 h, the longest period investigated. During this period, both CCW and CW intervals became progressively longer, increasing as much as threefold (Fig. 3A). However, the intervals varied in such a way that the fraction of time spent spinning CCW (the probability of spinning CCW) tended to remain constant (Fig. 3B). The probability of spinning CCW was chosen as a measure of the response because it has this stability. Rotational velocities also remained nearly constant. The cell shown in Fig. 3 averaged 10 Hz for the first hour, slowed to 7.5 Hz by the end of the second hour, and maintained that speed (to within ±0.5 Hz) for the remaining 4 h. Another cell increased its speed by about 30% over a comparable period. Variations in speed of other cells were smaller

than this. Changes in speed were not correlated with changes in rotational bias.

Behavior during exponential ramps. If the response of a cell is proportional to the rate of change of chemoreceptor occupancy, dP/dt, and a ramp of the form $C = C_{low} \exp(at)$ or $C = C_{high} \exp(-at)$ is switched on, then the response should shift by an amount proportional to a and remain nearly constant for the duration of the ramp. This behavior is shown in Fig. 4. The base-line fluctuations represent the normal statistical variation in rotational bias. When the ramps were turned on, the rotational bias changed rapidly to a new level, as predicted. The rate at which this level was established provides a measure of the time required by the cell to evaluate dP/dt. This time was relatively short, less than the mixing time constant, τ_{mix}. When the ramps were turned off, there was an overshoot in rotational bias that persisted for about 1 min, analogous to the overshoot observed during recovery from large-step stimuli, described earlier (6). With the exception of this period, the rotational bias faithfully mirrored changes in dP/dt, shown schematically at the bottom of each graph. To obtain a comparable change in rotational bias, down ramps had to be two to three times faster than up ramps, limiting the period of time during which data could be collected. Therefore, our conclusions for down ramps are more tentative.

The interval distributions remained exponentially distributed during up and down ramps. Results for up ramps of one particular rate are shown in Fig. 5. In this case, stimulation caused a slight decrease in the mean CW interval and a large increase in the mean CCW interval. The interval distributions remained exponential at all ramp rates tested, provided that the response did not saturate (data not shown).

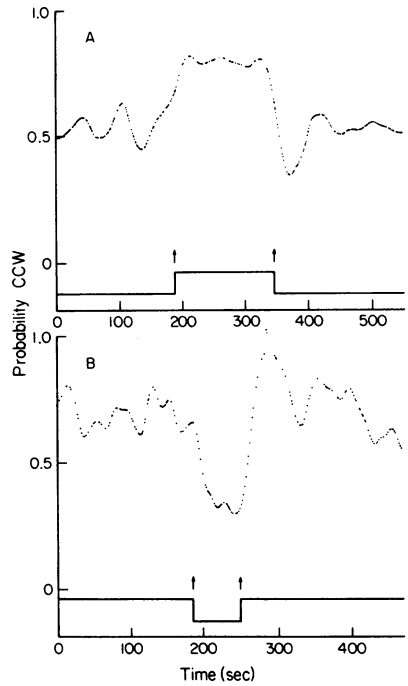

FIG. 4. Response of a typical cell to exponential ramps up or down. (A) Ramp from C_{low} to C_{high} at rate $a = 0.015\ s^{-1}$, beginning at $t = 177$ s and ending at $t = 339$ s. (B) Ramp from C_{high} to C_{low} at rate $a = -0.037\ s^{-1}$, beginning at $t = 184$ s and ending at $t = 248$ s. Arrows indicate times at which ramps began or ended at the flow cell. Changes in bias shown in the figure do not coincide precisely with the arrows, partly because of fluctuations in bias, partly because the spline smoothing spans a finite interval; see text.

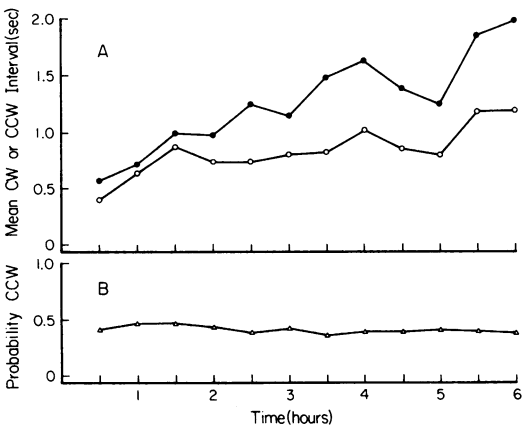

FIG. 3. Behavior of an adapted cell over a period of several hours. (A) Mean CW (○) and CCW (●) intervals. (B) Probability of spinning CCW (△). Each point shown was computed from data collected over a period of 3 to 5 min.

Figure 6 shows the changes in rotational bias observed as a function of ramp rate. Since there was a large variation in bias from cell to cell, these experiments were done with single cells. The responses of two cells to ramps up are shown in Fig. 6A, and the responses of one cell to ramps down are shown in Fig. 6B. The response threshold, i.e., the ramp rate required to cause a measurable change in bias from the unstimulated value, is relatively low for ramps up (Fig. 6A) but relatively high for ramps down (Fig. 6B). The slopes of the linear parts of these curves have roughly the same magnitude.

The lengths of both CW and CCW intervals changed during the ramps. For ramps up, CCW intervals lengthened, but CW intervals shortened. For ramps down, CCW intervals shortened, but CW intervals lengthened. During ramps up, CCW intervals were more sensitive to change than CW intervals: the relative increase

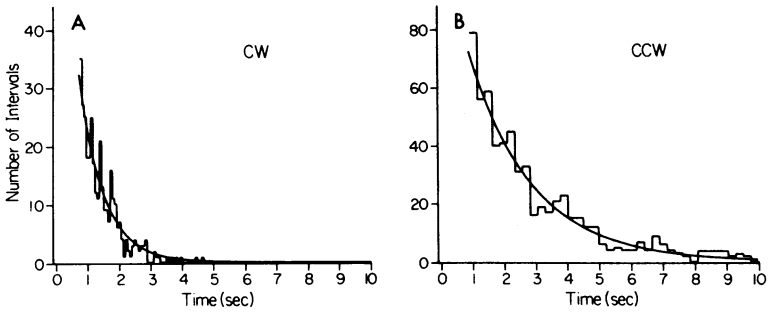

FIG. 5. CW and CCW interval distributions of cells during an exponential ramp up. Histograms for 13 records from six cells exposed to ramps of rate 0.013 s^{-1} were scaled, combined, and fit by exponentials, as described in the text. (A) CW interval distribution computed from 534 events longer than 0.4 s. Range of adjusted means for each record, 0.30 to 1.5 s; global adjusted mean, 0.69 s; decay time for the exponential fit, 0.78 s, reduced χ^2, 0.913; 17 degrees of freedom; *P* value, 56%. (B) CCW interval distribution computed from 795 events longer than 0.4 s; 32 events are off the scale. Range of adjusted means for each record, 0.75 to 12.0 s; global adjusted mean, 2.38 s; decay time for the exponential fit, 1.99 s; reduced χ^2, 1.18; 19 degrees of freedom; *P* value, 27%. (Not shown) CW and CCW interval distributions for the same cells before each ramp. CW global adjusted mean computed from 740 events longer than 0.04 s in 13 records, 0.76 s; CCW global adjusted mean computed from 948 events longer than 0.4 s in 13 records, 0.89 s. Exponential fits were not made to these data.

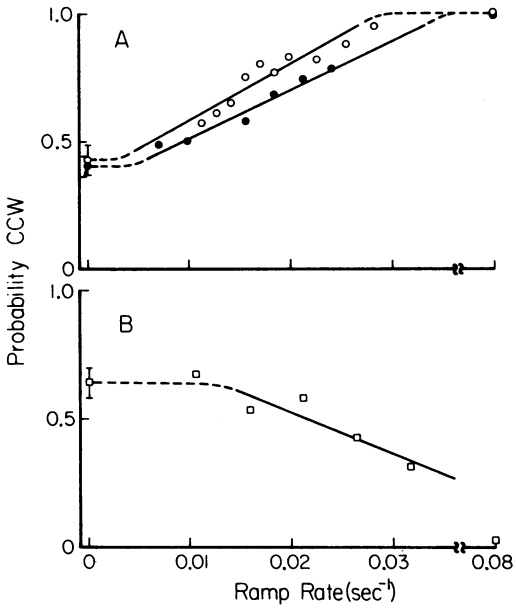

FIG. 6. Rotational bias as a function of ramp rate for exponential ramps up or down. Note the break in scale. (A) Responses of two cells to ramps up. The solid lines are least-squares fits to all but the first and last data points. The slopes of these lines are 21.5 ± 4.6 s (○) and 18.7 ± 4.1 s (●). The dashed lines were drawn by eye. The first data point, shown with error bars, represents the mean and standard deviation of the bias before the ramps. Values were 0.43 ± 0.06, 16 determinations (○); 0.41 ± 0.04, 12 determinations (●). The last data point was taken at the maximum rate attainable with the apparatus, at a time constant of about 12 s. (B) Responses of one cell to ramps down. Solid and dashed lines are as in (A). Slope of solid line, −16.0 ± 3.6 s; mean and standard deviation of first data point, 0.64 ± 0.06, 10 determinations.

in the mean CCW interval was greater than the relative decrease in the mean CW interval in virtually all cases (31 out of 34 ramps on a total of four cells). However, during ramps down, the relative increase in the mean CW interval was sometimes greater and sometimes smaller than the relative decrease in the mean CCW interval (CW increase greater in 12 out of 25 ramps on a total of eight cells). To obtain the results shown in Fig. 6, it was necessary to collect a large amount of data on a small number of cells, cells that remained tethered to the glass and continued to spin while subjected to flow over a period of several hours. One could learn more about relative changes in interval lengths by exposing a large number of cells to only a few ramps.

Behavior during exponentiated sine waves. The response to an exponentiated sine wave of intermediate frequency is shown in Fig. 7. At this frequency, the response is unsaturated, even at peak values of *dP/dt*. The response tracks *dP/dt*, not *P*; compare Fig. 7A and B. The response wave form is periodic but not quite sinusoidal, as expected from the up-down asymmetry noted in Fig. 6. The reversal rate leads *dP/dt* in phase, but only slightly (Fig. 7C).

Figure 8 is a Bode (log-log) plot of the amplitude of the response as a function of frequency. Such plots are widely used in the analysis of linear systems to determine response characteristics; linear domains with slopes of 20*n dB* per decade represent *n*th-order filters. The responses at the lowest frequencies (the first three data points) were lost in the noise owing to the normal statistical variation in base-line bias. At the highest frequencies, the cells spun exclusively CCW during the positive phase of the stimulus. The linear intermediate domain implies a

power-law dependence of amplitude on frequency; the value of the slope is indicative of a first-order high pass (adaptive) process; see Block et al. (8).

With increasing frequency, the base-line bias of the cells shifted in the CCW direction (data not shown). This is another consequence of the up-down asymmetry noted in Fig. 6. It would not occur were adaptation equally fast for changes on concentration in either direction. The response continued to track *dP/dt* at the highest frequencies tested.

DISCUSSION

Evidence for a bias regulator. The interval distributions shown in Fig. 2 and 5 and those obtained earlier with swimming cells (5, 9) or tethered cells (6, 8) can be fit accurately by single exponentials. This implies that reversals of the flagellar motors are generated by a Poisson process (6), a process with a constant probability per unit of time. The possibility remains that the distributions are nonexponential for times shorter than 0.4 s. There is some indication of this in data collected with the linear-graded filter apparatus; see Fig. 2A of reference 26. To find out, we need to use methods with even better time resolution.

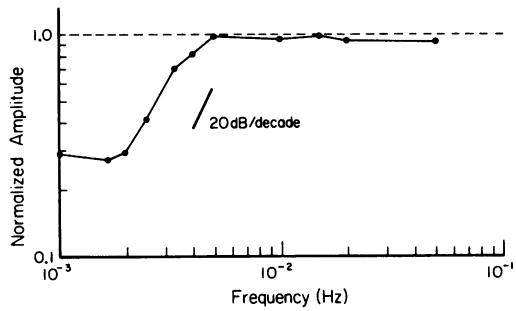

FIG. 8. Bode plot of response amplitude versus frequency for exponentiated sine waves. Concentration always varied between C_{low} and C_{high}. The peak-to-peak changes in rotational bias of two cells were normalized to the values obtained with saturating stimuli, averaged, and plotted as a function of frequency on a log-log scale. Reference line of slope 20 *dB* per decade (characteristic of a first-order high-pass filter) is shown for comparison.

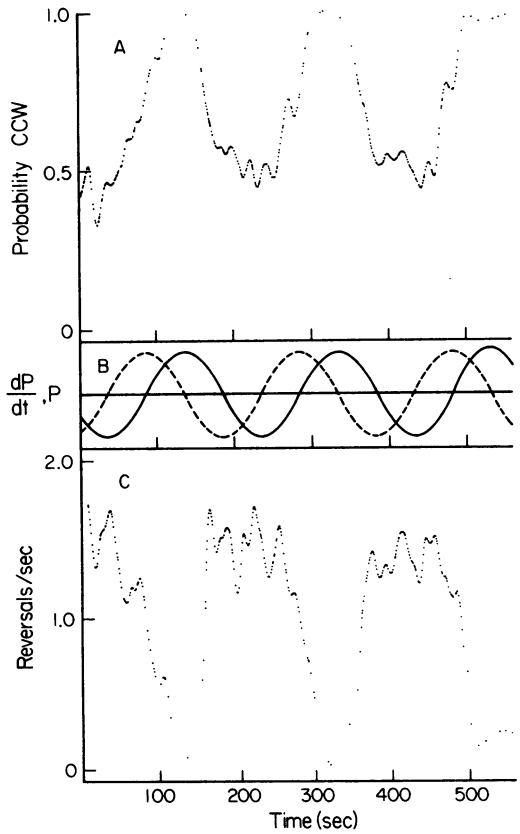

FIG. 7. Response of a cell to an exponentiated sine wave with a frequency of 0.005 Hz. Concentration varied from C_{low} to C_{high}. (A) Changes in rotational bias. Mean bias during this response was 0.71. Mean bias before stimulation was 0.64. (B) Changes in the fraction of receptor bound, *P*, (dashed line) and its time derivative, *dP/dt* (solid line). (C) Changes in reversal rate.

Two models that suggest mechanisms for the generation of spontaneous reversals are diagrammed in Fig. 9. The first is the response regulator model of Koshland (17, 18). As noted in Fig. 9A, it exploits the notion of a fluctuating intermediate to account for rotational transitions (18): "The steady-state level of response regulator (X_{ss}) varies in a Poissonian manner relative to a critical value (X_{crit}). When ($X_{ss} - X_{crit}$) is slightly less than zero, tumbling is generated. When ($X_{ss} - X_{crit}$) is greater than zero, smooth swimming results." Variations in which X_{ss} remains constant and X_{crit} fluctuates or in which both fluctuate also are acceptable. The model assumes that X is raised transiently when cells are exposed to an attractant; this leads to tumble suppression, which subsides when X returns to its original level. This model must be correct, a priori, in the sense that some signal controls the changes in rotational bias that occur during a chemotactic response; but, as we shall now show, variations in this signal do not generate exponential interval distributions.

The problem reduces to the question of how level crossings of such a regulator are distributed. Fluctuations expected in the amplitude of X are simply derived, but level-crossing (or zero-crossing) times are not (4). Many random functions have exponentially distributed amplitudes,

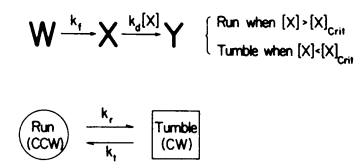

FIG. 9. Models for the generation of spontaneous reversals. (A) Response regulator model. An intermediate, X, is produced by one reaction and degraded by another. At steady state, the concentration of X is constant, on the average, but fluctuations occur. A mechanism exists that compares the instantaneous value of X with a reference level, X_{crit}. CCW intervals (runs) occur when X is larger than X_{crit}, and CW intervals (tumbles) occur when X is smaller than X_{crit}. (B) Two-state model. Two states, representing CCW rotation (a run) and CW rotation (a tumble), are connected by first-order rate constants k_r and k_t, which are the probabilities per unit of time of terminating these events. In the interest of using the common nomenclature, we assume a one-to-one correspondence between CCW intervals and runs (smooth segments in the track of a free-swimming cell) and CW intervals and tumbles (short erratic segments) (19). Exceptions occur in cells with an extreme CW bias, which can move in a slow quasi-smooth manner while rotating their flagella CW (16).

but very few have exponentially distributed zero crossings. We simulated the response regulator model by computer using a Montecarlo method. The histogram shown in Fig. 10 was obtained for the case of a cell whose average steady-state value $\langle X_{ss} \rangle = X_{crit} = 1{,}000$, with mean generation and destruction rates given by $\lambda = 1\ s^{-1}$. This histogram is not exponential; it has a very long tail, with some intervals lasting many thousands of seconds. The analytical solution, shown by the solid line, is derived in Appendix A. We also simulated cells with different rotational biases; i.e., with $\langle X_{ss} \rangle \neq X_{crit}$, or with X displaced relative to X_{crit}, as during a chemotactic response. These distributions were skewed but remained far from exponential (data not shown). Changes in the level of $\langle X_{ss} \rangle$ had virtually no effect on these results until $\langle X_{ss} \rangle \simeq 1$. With $\langle X_{ss} \rangle = 1$, the CW distribution was exponential, but the CCW distribution was not. An exponential distribution for CW intervals is obtained when $\langle X_{ss} \rangle = 1$ because CW rotation occurs only for one state ($X = 0$), and the probability per unit of time of leaving this state is constant. This feature is exploited for both rotational modes in the two-state model (8).

The exponential fits to the data shown in Fig. 2 and 5 all map onto the dashed line shown in Fig. 10. The long intervals predicted by the response regulator model are not observed. Note (Appendix A) that this distribution has a tail that decays as $t^{-3/2}$, which cannot be fit by an exponential. Thus, we can rule out mechanisms in which flagellar reversals are generated by level crossings.

In the two-state model (Fig. 9B), transitions between binary states occur with constant probability per unit of time and yield exponential distributions for either state, with mean lifetimes given by $1/k_r$ and $1/k_t$. These states might represent alternate conformations of a protein, occupancies of a receptor, or the like. In the absence of chemotactic stimulation, both k_r and k_t can drift with time, as indicated in Fig. 3A, but in this case they do so proportionately, so that the function $k_t/(k_r + k_t)$, the fraction of time spent spinning CCW, remains approximately constant (Fig. 3B). The drift shown in Fig. 3A cannot be explained by a reduction in proton motive force, which has been found to lengthen CCW intervals and shorten CW intervals (15), i.e., to decrease k_r and increase k_t. The data given in the legend of Fig. 5 indicate that the chemotactic signal shifts k_r and k_t in opposite directions, but not by a proportionate amount; k_r changes by more than k_t. The chemotactic signal may well be an intermediate, X, of the sort envisaged by Koshland (17, 18), but it controls the bias of the flagellar motors, not individual transition times; therefore, we refer to it as a bias regulator. In the two-state model, fluctuations in X become largely irrelevant.

Evidence for proportional control. We have found that the change in bias is a function of the time rate of change of chemoreceptor occupancy, dP/dt (Fig. 4). This function is linear over a wide range, except for a small threshold seen for ramps up (Fig. 6A) and a larger threshold seen for ramps down (Fig. 6B). The magnitudes of the slopes of the linear portions of these curves, which relate to the gain of the system, are not as different as might have been expected, given the marked asymmetry in rates of adaptation to large-step stimuli (6); however, they are consistent with predictions based on measurements of responses to impulse and small-step stimuli (8; unpublished results). Results obtained when dP/dt was varied sinusoidally (Fig. 7) confirm that the response depends on dP/dt, not on P itself. The data summarized in Fig. 8, although consistent with those of Fig. 6, are of limited value because of the up-down asymmetry and saturation. Because the relative phase of the response was not observed to vary as the frequency increased (data not shown), the high-frequency cutoff, apparent in Fig. 8, must result from saturation, not from a limit set by any characteristic adaptation time. As noted earlier (Fig. 4), this time is of the same order of magnitude as the mixing time constant (11 s) or less. We know from measurements of the impulse response that the longest time constant operative in wild-type cells in the small-signal domain is about 4 s (8).

How can the cell generate a response proportional to the time rate of change of chemoreceptor occupancy? Somehow it must make a running comparison between the present chemoreceptor occupancy, P, and the occupancy in the recent past. A comparison of this kind was proposed in a theory developed some years ago by Delbrück and Reichardt to explain light adaptation in *Phycomyces* spp. (12). Expressed in language appropriate to chemotaxis, this theory asserts that an internal variable, A, representing the virtual occupancy to which a cell is adapted, changes at a rate proportional to an error signal $(P - A)$. Formally: $dA/dt = (P - A)/\tau$, where τ is an adaptation time constant. In general, A will track P but will be filtered by a time constant τ. When $A = P$, $dA/dt = 0$, and the cell is fully adapted. Consider, for example, the case in which P is first held constant and then increased at a constant rate, a. A lags P by an increasing amount for the first few time constants, until $(P - A)$ reaches $a\tau$, after which $(P - A)$ remains constant. Thus, the main features of the ramp experiments can be explained if the change in rotational bias is proportional to the error signal $(P - A)$. If this is so, the change in bias is proportional to the ramp rate, a.

The level of adaptation, A, is equivalent to the receptor occupancy averaged over the past with a weighting factor (memory) that decays exponentially with time; see Appendix B. Information about receptor occupancy is relevant only if it is recent on the scale of the time constant, τ. In general, the memory of the cell cannot be characterized by a single exponential; however, when changes in concentration occur at low enough frequency, it can be: the system behaves as a first-order high-pass filter (8). The gradual changes imposed in the ramp experiments fall in this low-frequency domain.

The Delbrück-Reichardt model does not account for the response thresholds evident in Fig. 6. A biochemically explicit model that can do so is outlined in Appendix C. In this model, the biochemical correlate for A is the level of methylation of a methyl-accepting chemotaxis protein, which, in the case of α-methylaspartate, is also the receptor (30; for a review, see 27). The error signal is generated by an imbalance between receptor occupancy and methylation. This signal controls both the behavior of the flagellar motors and, via a feedback loop, the activities of the methylation enzymes. Nonlinearities in this activation produce response thresholds.

Data obtained earlier with large-step stimuli were explained by assuming that adaptation occurs at a constant rate (6). In the model described in Appendix C, this happens when the methylation enzymes are fully activated. Adaptation to large downward steps in the concentration of α-methylaspartate is much faster than adaptation to upward steps (6). This appeared to explain the asymmetry observed when cells were tracked in spatial gradients of aspartate, in which changes in run length were much larger when cells swam up the gradients than when they swam down the gradients (5). The data shown in Fig. 6 suggest that these differences are due instead to an asymmetry in response thresholds.

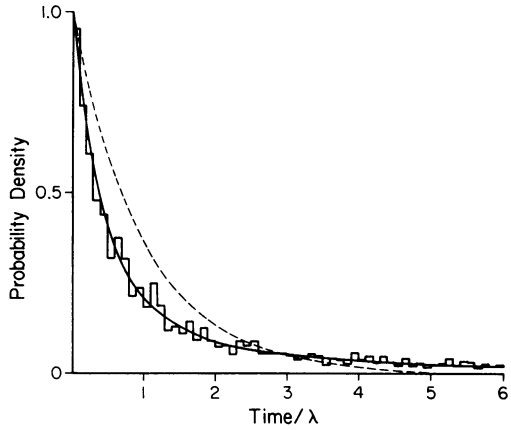

FIG. 10. Interval distribution predicted by the response regulator model (solid line) compared with an exponential distribution of the same area (dashed line). The solid line is the analytical solution given by equation A6. The histogram is the result of a Monte-carlo simulation. We assumed an average steady-state concentration $\langle X_{ss} \rangle = 1{,}000 = X_{crit}$, corresponding to a probability CCW = 0.5, and that X is generated at a rate $k_f = 1\ s^{-1}$ and destroyed at a rate $k_d = 0.001\ s^{-1}$, yielding a mean flux $\lambda = 1\ s^{-1}$. Some 23% of the events predicted by the analytical solution and found in the simulation are off the scale, as compared with 0.3% for the exponential distribution. The mean interval predicted by the analytical solution is infinite. The longest interval found in the simulation was 5,985 s.

The overshoots that occur when ramps are switched off (Fig. 4) are not explained by the models presented. These overshoots, although of smaller magnitude than those seen earlier during recovery from large step changes in the concentration of attractants or repellents (6), last for similar times. In both sets of experiments the cells sustain a monotonic change in bias for a relatively long period of time. It is likely that an intermediate accumulates during this time that affects the rotational bias when adaptation is nearly complete. One candidate for this intermediate is an incorrectly methylated or demethylated methyl-accepting chemotaxis protein, i.e., one that signals the presence of chemoattractants other than the one used as a stimulus.

General conclusions. Distributions of CW and

CCW intervals remain exponential, even when cells are subject to continuous chemotactic stimulation. This behavior implies that transitions between motor states occur at random, at rates controlled by signals whose amplitudes depend on sensory input. Adaptation to changes in concentration occurs via proportional control: the signal that determines the transition rates is proportional to the difference between current and past receptor occupancy. This control can be imposed by biochemical pathways that involve negative feedback.

APPENDIX A

Mathematical analysis of a response regulator model. Consider the model diagrammed in Fig. 9A. The problem is to derive the probability distribution functions for intervals when X is above (or below) X_{crit}. For simplicity, we examine the case in which $X > X_{crit}$ exactly half the time, on the average. Symmetry then requires that $X_{crit} = \langle X_{ss} \rangle$, the average steady-state level of X. At steady state, $\langle X_{ss} \rangle = k_f/k_d$. If the value of X is reasonable (say, 100 or greater), then fluctuations in the amplitude of X will be given by a Gaussian distribution with spread proportional to $\sqrt{X}$. In this case, the flux out of state X varies only slightly, and we can treat the fluxes which create and destroy X as essentially constant. The probability density function for the creation of X is given by $\lambda e^{-\lambda t}$, with $\lambda = k_f$. An identical relation holds for the destruction of X.

The problem may be thought of as a series of successive events in which the number of X molecules (i.e. the concentration X) is increased or decreased by 1. These events describe a random walk in the concentration X. Let X start at $\langle X_{ss} \rangle$. The probability density function for the times of excursions of X below (or above) $\langle X_{ss} \rangle$ will be given by the convolution

$$\rho(t) = \sum_{k=1}^{\infty} p_k g_k(t) \qquad \text{(A1)}$$

where p_k is the probability that a random walk over the integers, starting at 0, will reach the value 1 in exactly k steps (known as a first passage time) and $g_k(t)$ is the probability density function which represents the distribution of the sum of k separate times, each drawn from an exponential distribution, i.e., the density function for the time it takes to make k steps. The probability p_k is given by

$$p_k = \frac{1}{k} \begin{pmatrix} k \\ \frac{k+1}{2} \end{pmatrix} 2^{-k} \qquad \text{(A2)}$$

where k is an odd integer (13). Now, $g_k(t)$ is a probability density representing the sum of times, each of which will be distributed with exponential density $h(t)$. Since an event (a change in X) arises as a result of one of two concurrent Poisson processes (X is created or destroyed), these events will be distributed as $h(t) = 2\lambda e^{-2\lambda t}$. Therefore, by the convolution theorem, $g_k(t)$ is the k-fold convolution of $h(t)$ with itself. This convolution yields the gamma distribution

$$g_k(t) = \frac{(2\lambda)^k t^{k-1} e^{-2\lambda t}}{\Gamma(k)} \qquad \text{(A3)}$$

Insertion of these expressions into equation A1 yields

$$\rho(t) = \sum_{k \text{ odd}} \frac{1}{k} \begin{pmatrix} k \\ \frac{k+1}{2} \end{pmatrix} \frac{\lambda^k t^{k-1} e^{-2\lambda t}}{(k-1)!} \qquad \text{(A4)}$$

which, after some manipulation, can be reduced to a form representing a standard series (23):

$$\rho(t) = \frac{e^{-2\lambda t}}{t} \sum_{r=0}^{\infty} \frac{(\lambda t)^{r+1}}{r!(r+1)!} \qquad \text{(A5)}$$

Equation A5 is equivalent to

$$\rho(t) = \frac{e^{-2\lambda t} I_1(2\lambda t)}{t} \qquad \text{(A6)}$$

where I_1 is a modified Bessel function of the first kind. This density function is shown as the solid line in Fig. 10. Equation A6 is actually a special case of the general formula for the distribution of first-passage times in a birth and death process (a so-called queuing problem) in which events occur with fixed probability (3). For short times, $\rho(t)$ decays rapidly as $e^{-2\lambda t}$; for long times, it decays slowly as $t^{-3/2}$. The integral of $\rho(t)$ can be calculated by recourse to standard forms. As expected for a probability distribution, the area equals 1; however, the slowness of the decay for large t gives an expectation value for t that is infinite. This kind of counter-intuitive behavior is common for certain types of random walks and represents the fact that lead changes occur surprisingly infrequently, even in games with balanced odds. For example, in a coin-tossing game with balanced stakes and a fair coin tossed n times, the average lead for one or the other player increases roughly as n (13). Therefore, as n goes to infinity, the length of the average lead does also, and so the expectation value for a lead is infinite.

APPENDIX B

Equivalent statements of a model for adaptation. The version of the Delbrück-Reichardt model presented in the text contains two assumptions about the behavior of the system. (i) The response, R, is proportional to an error signal

$$R = g(P - A) \qquad \text{(B1)}$$

where g is a constant of proportionality specifying the gain, P is the receptor occupancy, and A is an adaptation level. (ii) A follows P according to the first-order differential equation

$$dA/dt = (P - A)/\tau \qquad \text{(B2)}$$

where τ is an adaptation time constant. The variable A can be eliminated from these equations by solving equation B2 for A and substituting the result into equation B1. The solution of equation B2 for $t \gg \tau$ is

$$A(t) = \frac{e^{-t/\tau}}{\tau} \int_0^t P(t') e^{t'/\tau} \, dt' \qquad \text{(B3)}$$

which can be rewritten and substituted into equation B1 to yield

$$R(t) = g\left[P(t) - \frac{1}{\tau} \int_0^t P(t') e^{-(t-t')/\tau} \, dt' \right] \qquad \text{(B4)}$$

The first term in the brackets, $P(t)$, is the current receptor occupany. The second term is an average of P over past times with a weighting factor that decays exponentially with time. The response is proportional to the difference of these terms.

APPENDIX C

Model for adaptation that can account for response thresholds. We make the usual assumption that the signal generated when an attractant binds a receptor is switched off when the receptor is methylated (27). We identify P (equation B1) with the fraction of receptors that have bound attractant and A with the fraction of receptors that have bound attractant and are methylated. If the total number of receptors is N_0, then the number that have bound attractant but are not methylated is $(P - A)\ N_0$, which we call S (for signal). Methylation of S is carried out by a methyltransferase; let the total number of these molecules be M_0. We assume that the enzyme is activated by the error signal (or the response), e.g., by association with a ligand $L = fS$, where f is a feedback constant. This reaction sequence comprises a negative feedback loop: if S increases, L increases; more M is activated, and S decreases.

The Delbrück-Reichardt model follows when the feedback is proportional to the signal. If M is activated by association with L, i.e., if

$$M + L \rightleftharpoons M^* \qquad \text{(C1)}$$

where M is the number of free enzyme molecules and M^* is the number bound to L, then

$$M^* = LM_0/(K_d + L) \qquad \text{(C2)}$$

where K_d is the dissociation constant for the enzyme-ligand complex. For $L \ll K_d$, $M^* = fSM_0/K_d$, and activation is proportional to the signal. We assume that methylation proceeds by Michaelis-Menten kinetics, i.e., at a rate

$$kM^*S/(K_m + S) \qquad \text{(C3)}$$

where k is the rate constant for conversion of the enzyme-substrate complex to enzyme and product and K_m is the Michaelis-Menten constant. Now, in the middle of an up ramp, the response is constant; therefore, S is constant. The rate at which the receptor is methylated (equation C3) must be equal to the rate at which additional attractant is bound to the receptor; since $dP/dt = a/4$, this quantity is $(a/4)\ N_0$:

$$kM^*S/(K_m + S) = aN_0/4 \qquad \text{(C4)}$$

Substituting the relation $L = fS$ and equation C2 into equation C4 gives a quadratic in S which can be solved to yield S as a function of a. If $L \ll K_d$ and $S \gg K_m$, S is proportional to a, as required. If $L \gg K_d$, $M^* = M_0$, and methylation occurs at a constant rate. In this limit, the response saturates (equation B1 breaks down), and S is not proportional to a.

A response threshold arises when there is some methyltransferase activity even at very low levels of S. This allows the cell to adapt without generating a sizable error signal. This hypothesis is plausible, given the turnover of methyl groups that occurs in the absence of stimulation (14). To cite an extreme example, suppose that some of the methyltransferase, M', is active even in the absence of ligand, i.e., that

$$M^* = M' + LM_0/(K_d + L) \qquad \text{(C5)}$$

where M_0 now is the total number of molecules subject to activation and inactivation. For $L \ll K_d$, $M^* = M' + fSM_0/K_d$, and equation C4 leads to an expression that predicts a response threshold of order $a = 4kM'/N_0$. An alternative possibility is that more than one molecule of L binds to M but that activation owing to binding of the second or subsequent ligands is relatively less effective. Such an allosteric interaction would introduce the necessary nonlinearity.

In a more realistic model, methylation would be offset by demethylation, and the signal S would activate the methyltransferase and inactivate the methylesterase. Differences in thresholds for up ramps and down ramps then could be accounted for by differences in the activation of these two enzymes.

ACKNOWLEDGMENTS

We thank Gary Lorden for consultations on probability theory, Robert Smyth for providing the cubic spline-fit routine, and Greg Matthews for digitizing.

This work was supported by Public Health Service grant AI 16478 from the National Institute of Allergy and Infectious Diseases. S.M.B. and J.E.S. acknowledge support as National Science Foundation predoctoral fellows during some of this work.

LITERATURE CITED

1. **Adler, J.** 1973. A method for measuring chemotaxis and use of the method to determine optimum conditions for chemotaxis by *Escherichia coli*. J. Gen. Microbiol. **74**:77–91.
2. **Armstrong, J. B., J. Adler, and M. M. Dahl.** 1967. Nonchemotactic mutants of *Escherichia coli*. J. Bacteriol. **93**:390–398.
3. **Bailey, N. T.** 1964. The elements of stochastic processes, ch. 11. John Wiley & Sons, Inc., New York.
4. **Bendat, J. S.** 1958. Principles and applications of random noise theory, ch. 10. John Wiley & Sons, Inc., New York.
5. **Berg, H. C., and D. A. Brown.** 1972. Chemotaxis in *Escherichia coli* analysed by three-dimensional tracking. Nature (London) **239**:500–504.
6. **Berg, H. C., and P. M. Tedesco.** 1975. Transient response to chemotactic stimuli in *Escherichia coli*. Proc. Natl. Acad. Sci. U.S.A. **72**:3235–3239.
7. **Bevington, P. R.** 1969. Data reduction and error analysis for the physical sciences, ch. 11. McGraw-Hill Book Co., New York.
8. **Block, S. M., J. E. Segall, and H. C. Berg.** 1982. Impulse responses in bacterial chemotaxis. Cell **31**:215–226.
9. **Brown, D. A., and H. C. Berg.** 1974. Temporal stimulation of chemotaxis in *Escherichia coli*. Proc. Natl. Acad. Sci. U.S.A. **71**:1388–1392.
10. **Dahlquist, F. W., R. A. Elwell, and P. S. Lovely.** 1976. Studies of bacterial chemotaxis in defined concentration gradients. J. Supramol. Struct. **4**:329–342.
11. **Dahlquist, F. W., P. Lovely, and D. E. Koshland, Jr.** 1972. Quantitative analysis of bacterial migration in chemotaxis. Nature (London) New Biol. **236**:120–123.
12. **Delbrück, M., and W. Reichardt.** 1956. System analysis for the light growth reactions of *Phycomyces*, p. 3–44. *In* D. Rudnick (ed.), Cellular mechanisms in differentiation and growth. Princeton University Press, Princeton, N.J.
13. **Feller, W.** 1968. An introduction to probability theory and its applications, vol. 1, ch. 3. John Wiley & Sons, Inc., New York.
14. **Goy, M. F., M. S. Springer, and J. Adler.** 1977. Sensory transduction in *Escherichia coli*: role of a protein methylation reaction in sensory adaptation. Proc. Natl. Acad.

Sci. U.S.A. 74:4964–4968.
15. **Khan, S., and R. M. Macnab.** 1980. The steady-state counterclockwise/clockwise ratio of bacterial flagellar motors is regulated by protonmotive force. J. Mol. Biol. 138:563–597.
16. **Khan, S., R. M. Macnab, A. L. DeFranco, and D. E. Koshland, Jr.** 1978. Inversion of a behavioral response in bacterial chemotaxis: explanation at the molecular level. Proc. Natl. Acad. Sci. U.S.A. 75:4150–4154.
17. **Koshland, D. E., Jr.** 1977. A response regulator model in a simple sensory system. Science 196:1055–1063.
18. **Koshland, D. E., Jr.** 1980. Bacterial chemotaxis as a model behavioral system, p. 64–68. Raven Press, New York.
19. **Larsen, S. H., R. W. Reader, E. N. Kort, W.-W. Tso, and J. Adler.** 1974. Change in direction of flagellar rotation is the basis of the chemotactic response in *Escherichia coli*. Nature (London) 249:74–77.
20. **Macnab, R. M., and D. E. Koshland, Jr.** 1972. The gradient-sensing mechanism in bacterial chemotaxis. Proc. Natl. Acad. Sci. U.S.A. 69:2509–2512.
21. **Mesibov, R., and J. Adler.** 1972. Chemotaxis toward amino acids in *Escherichia coli*. J. Bacteriol. 112:315–326.
22. **Mesibov, R., G. W. Ordal, and J. Adler.** 1973. The range of attractant concentrations for bacterial chemotaxis and the threshold and size of response over this range. J. Gen. Physiol. 62:203–223.
23. **Olver, F. W.** 1968. Bessel functions of integer order, p. 358–433. *In* M. Abramowitz and I. A. Stegun (ed.), Handbook of mathematical functions. Dover Publications, Inc., New York.
24. **Reinsch, C. H.** 1967. Smoothing by spline functions. Numerische Mathematik 10:177–183.
25. **Reinsch, C. H.** 1971. Smoothing by spline functions II. Numerische Mathematik 16:451–454.
26. **Segall, J. E., M. D. Manson, and H. C. Berg.** 1982. Signal processing times in bacterial chemotaxis. Nature (London) 296:855–857.
27. **Springer, M. S., M. F. Goy, and J. Adler.** 1979. Protein methylation in behavioural control mechanisms and in signal transduction. Nature (London) 280:279–284.
28. **Spudich, J. L., and D. E. Koshland, Jr.** 1975. Quantitation of the sensory response in bacterial chemotaxis. Proc. Natl. Acad. Sci. U.S.A. 72:710–713.
29. **Tsang, N., R. Macnab, and D. E. Koshland, Jr.** 1973. Common mechanism for repellents and attractants in bacterial chemotaxis. Science 181:60–63.
30. **Wang, E. A., and D. E. Koshland, Jr.** 1980. Receptor structure in the bacterial sensing system. Proc. Natl. Acad. Sci. U.S.A. 77:7157–7161.